Atmos. Chem. Phys., 16, 11823–11836, 2016
www.atmos-chem-phys.net/16/11823/2016/
doi:10.5194/acp-16-11823-2016

Atmospheric Chemistry and Physics Open Access EGU

Heterogeneous photochemistry of imidazole-2-carboxaldehyde: HO_2 radical formation and aerosol growth

Laura González Palacios[1,2], Pablo Corral Arroyo[3,4], Kifle Z. Aregahegn[6,a], Sarah S. Steimer[3,5,b], Thorsten Bartels-Rausch[3], Barbara Nozière[6], Christian George[6], Markus Ammann[3], and Rainer Volkamer[1,2]

[1]Department of Chemistry and Biochemistry, 215 UCB, University of Colorado, Boulder, CO 80309, USA
[2]Cooperative Institute for Research in Environmental Sciences (CIRES), 216 UCB, University of Colorado, Boulder, CO 80309, USA
[3]Laboratory of Environmental Chemistry, Paul Scherrer Institute, 5232 Villigen, Switzerland
[4]Department of Chemistry and Biochemistry, University of Bern, 2012 Bern, Switzerland
[5]Institute for Atmospheric and Climate Science, Swiss Federal Institute of Technology Zurich, 8092 Zurich, Switzerland
[6]Université Lyon 1, CNRS, UMR 5256, IRCELYON, Institut de recherches sur la catalyse et l'environnement de Lyon, 2 avenue Albert Einstein, 69626 Villeurbanne, France
[a]now at: Chemistry Department, University of California, Irvine, California, 92697-202, USA
[b]now at: Department of Chemistry, University of Cambridge, Cambridge, CB2 1EW, UK

Correspondence to: Rainer Volkamer (rainer.volkamer@colorado.edu)

Received: 1 February 2016 – Published in Atmos. Chem. Phys. Discuss.: 11 February 2016
Revised: 29 June 2016 – Accepted: 15 July 2016 – Published: 23 September 2016

Abstract. The multiphase chemistry of glyoxal is a source of secondary organic aerosol (SOA), including its light-absorbing product imidazole-2-carboxaldehyde (IC). IC is a photosensitizer that can contribute to additional aerosol ageing and growth when its excited triplet state oxidizes hydrocarbons (reactive uptake) via H-transfer chemistry. We have conducted a series of photochemical coated-wall flow tube (CWFT) experiments using films of IC and citric acid (CA), an organic proxy and H donor in the condensed phase. The formation rate of gas-phase HO_2 radicals (P_{HO_2}) was measured indirectly by converting gas-phase NO into NO_2. We report on experiments that relied on measurements of NO_2 formation, NO loss and HONO formation. P_{HO_2} was found to be a linear function of (1) the [IC] × [CA] concentration product and (2) the photon actinic flux. Additionally, (3) a more complex function of relative humidity ($25\,\% < RH < 63\,\%$) and of (4) the O_2 / N_2 ratio ($15\,\% < O_2 / N_2 < 56\,\%$) was observed, most likely indicating competing effects of dilution, HO_2 mobility and losses in the film. The maximum P_{HO_2} was observed at 25–55 % RH and at ambient O_2 / N_2. The HO_2 radicals form in the condensed phase when excited IC triplet states are reduced by H transfer from a donor, CA in our system, and subsequently react with O_2 to regenerate IC, leading to a catalytic cycle. OH does not appear to be formed as a primary product but is produced from the reaction of NO with HO_2 in the gas phase. Further, seed aerosols containing IC and ammonium sulfate were exposed to gas-phase limonene and NO_x in aerosol flow tube experiments, confirming significant P_{HO_2} from aerosol surfaces. Our results indicate a potentially relevant contribution of triplet state photochemistry for gas-phase HO_2 production, aerosol growth and ageing in the atmosphere.

1 Introduction

The sources and sinks of radicals play an important role in the oxidative capacity of the atmosphere. Radicals and other oxidants initiate the chemical degradation of various trace gases, which is key in the troposphere (Jacob, 1999). The hydroxyl (OH) and peroxyl (HO_2) radicals belong to the HO_x chemical family and are primarily generated by ultraviolet radiation photochemical reactions (Calvert and Pitts, 1966), like the reaction of $O(^1D)$ (from O_3) with H_2O or photolysis of HONO, HCHO, H_2O_2 or acetone. Some secondary gas-phase sources are the ozonolysis of alkenes or $O(^1D) + CH_4$

(Monks, 2005). The oxidation of volatile organic compounds (VOCs) by OH and other oxidants in the presence of NO leads to perturbations in the HO_x, NO_x and RO_x radical cycles that affect O_3 and aerosol formation (Monks, 2005; Sheehy et al., 2010). The kinetics and photochemical parameters of these reactions are relatively well-known in the gas phase (Atkinson et al., 2004; Sander et al., 2011). However, this does not apply to the sources and sinks for HO_x in atmospheric droplets and on aerosol surfaces (Ervens et al., 2011). Uptake of OH from the gas phase and H_2O_2 photolysis in the condensed phase are the primary known sources for HO_x in the condensed phase. HO_2 is highly soluble and the concentrations of OH, the most effective oxidant in the condensed phase, depend on HO_2 radicals. Another source of HO_x radicals is from the chemical reactions of reduced metal ions and H_2O_2, known as Fenton reactions (Fenton, 1894; Deguillaume et al., 2005). Direct photolysis of H_2O_2, nitrite, nitrate (Zellner et al., 1990), hydroperoxides (Zhao et al., 2013) and light-absorbing secondary organic aerosol (SOA) (Badali et al., 2015) are also sources of HO_x in the condensed phase. Other studies have shown that the photochemistry of iron (III) oxalate and carboxylate complexes, present in aqueous environments (e.g., wastewater, clouds, fogs, particles), can initiate a radical chain reaction serving as an aqueous source of HO_2 and Fe^{2+}. Fe^{2+} can then regenerate OH starting a new cycle of Fenton reactions (Weller et al., 2013a, b). The temperature-dependent rate constants of OH in the aqueous phase have been studied for a limited subset of organics (Ervens et al., 2003). However, there is still a wide gap with respect to understanding the sources, sinks, kinetics and photochemical reaction pathways of HO_x radicals in the condensed phase (George et al., 2015).

Our study investigates photosensitizers as an additional HO_x source that may be relevant to further modify RO_x and NO_x reaction cycles in both the condensed and gas phases. It is motivated by the formation of superoxide in terrestrial aqueous photochemistry (Draper and Crosby, 1983; Faust, 1999; Schwarzenbach et al., 2002), by more recent observations that irradiated surfaces containing titanium dioxide generate HO_x radicals in the gas phase (Yi et al., 2012) and by the generation of OH from metal oxides acting as photocatalysts in mineral dust (Dupart et al., 2012). Past studies have demonstrated the reactivity of glyoxal towards ammonium ions and amines as a source for light-absorbing brown carbon (Nozière et al., 2009; Galloway et al., 2009; Shapiro et al., 2009; Kampf et al., 2012). One of these products is imidazole-2-carboxaldehyde (IC; Galloway et al., 2009), which absorbs light at UV wavelengths ($\lambda < 330$ nm) (Maxut et al., 2015). Other imidazole-type compounds and light-absorbing products are formed in minor amounts but can nonetheless impact optical and radiative properties of secondary organic aerosols (SOAs; Sareen et al., 2010; Trainic et al., 2011). Photochemical reactions by these species are not typically accounted for in models yet but have a possible role for SOA formation and aerosol aging mechanisms (Sumner et al., 2014).

Photosensitizers are light-absorbing compounds that absorb and convert the energy of photons into chemical energy that can facilitate reactions, e.g., at surfaces or within aerosols (George et al., 2015). For example, aerosol seeds containing humic acid or 4-(benzoyl)benzoic acid (4-BBA), two other known photosensitizers, can induce the reactive uptake of VOCs when exposed to light, leading to SOA formation (Monge et al., 2012). Aregahegn et al. (2013) and Rossignol et al. (2014) suggested a mechanism for autophotocatalyic aerosol growth, where radicals are produced from the reaction of an H-donor hydrocarbon species, in this case limonene, and the triplet state of IC. The condensed-phase citric acid and the gas-phase limonene are H-atom donors (in this article we refer to them as H donors) rather than proton donors as in the case of a Brønsted acid. In particular, the transfer of the H atom leads to the formation of an alkyl-radical species. The H-atoms transfer thus has the same effect as an H-atom abstraction reaction by Cl or OH radicals.

Field measurements on fog water samples confirmed that triplet excited states of organic compounds upon irradiation can oxidize model samples such as syringol (a biomass burning phenol) and methyl jasmonate (a green leaf volatile), accounting for 30–90 % of their loss (Kaur et al., 2014). There are very few field measurements of imidazoles; a recent study by Teich et al. (2016) identified five imidazoles (1-butylimidazole, 1-ethylimidazole, 2-ethylimidazole, IC and 4(5)-methylimidazole) in ambient aerosols in concentrations ranging from 0.2 to 14 ng m^{-3}. IC, the molecule of interest in this study, was measured in its hydrated form in ambient aerosols in three urban areas with signs of air pollution and biomass burning (Leipzig, Germany; Wuqing and Xianghe, China). The observed quantities of hydrated IC ranged from 0.9 to 3.2 ng m^{-3}. The authors claim that these values could be a lower limit due to high losses of IC during sample preparation indicated by low recovery from standard solutions. This suggests that IC and other imidazole derivatives are present in areas with high pollution and biomass burning. Field measurements in Cyprus during the CYPHEX campaign in 2014 detected IC and bis-imidazole in ambient aerosol samples (Jacob, 2015). The IC diurnal cycles showed the highest concentrations at night (0.02–0.115 ng m^{-3}) and lower concentrations during the day, suggesting that ambient concentrations of IC in aerosols are a balance between photochemical sources and sinks. Imidazoles seem to be widespread in polluted and remote areas. However, the atmospheric implications of IC as a photosensitizer, a proxy species of brown carbon light absorption, and as a radical source in ambient aerosols remains unclear.

The existence of such photocatalytic cycles could be of atmospheric significance. Indeed, Canonica et al. (1995) suggested that the initial carbonyl, triggering the photochemical properties, is regenerated via a reaction with oxygen-producing HO_2. To our knowledge, the production of such

radical side products has not been investigated under atmospheric conditions previously. We therefore report here on the HO_2 radical production from IC in the condensed phase.

2 Experimental section

A series of flow tube experiments were conducted to investigate the formation of gas-phase HO_2 radicals from IC photochemistry using two different coated-wall flow tube (CWFT) reactors (Sect. 2.1). Section 2.2 describes aerosol flow tube experiments that confirm the photochemical production of HO_2 radicals in the absence of other known gas-phase radical sources in aerosols. All experiments were performed at atmospheric pressure.

2.1 Coated-wall flow tube experiments

The CWFT experiments were designed to investigate the gas-phase production of HO_2 radicals from a film containing IC and citric acid (CA) matrix as a function of UV light intensity, IC concentration in the film, relative humidity (RH) and O_2 mixing ratio. Two similar experimental setups were used as shown in Fig. 1. Some of the differences, not major, consist in the flow-reactor volume, surface area, flow rates, IC mass loading, NO mixing ratio, temperature inside the reactor and the connected instrumentation.

Setup 1. Experiments were conducted in a photochemical flow system equipped with a Duran glass CWFT (0.40 cm inner radius, 45.2 and 40.0 cm length, 113.6 and 100.4 cm^2 inner surface, surface-to-volume ratio (S / V) = 5.00 cm^{-1}), which was housed in a double-jacketed cell coupled to a recirculating water bath to control the temperature at 298 K; the setup is shown in Fig. 1a. A thin film of IC + CA was deposited inside the tubular glass flow tube. The experimental procedure for the preparation of the films is described in Sect. 2.1.2. The system consisted of seven ultraviolet lamps (UV-A range, Philips Cleo Effect 22 W: 300–420 nm, 41 cm, 2.6 cm o.d.) surrounding the flow tube in a circular arrangement of 10 cm in diameter.

Setup 2. The second CWFT (CWFT 0.60 cm inner radius, 50 cm length, inner surface 188.5 cm^2, S/V = 3.33 cm^{-1}) reactor had a glass jacket to allow water to circulate and maintain temperature control inside the tube at 292 K. The coated-wall tubes were snugly fit into the CWFT as inserts. The CWFT was surrounded by the same seven fluorescent lamps as in Setup 1. The light passed through different circulating water cooling jackets for both setups, thus providing a different light path for each setup.

Setup 1 and 2. The actinic flux in the flow tube reactor, $F_{FT}(\lambda)$, was measured by actinometry of NO_2 (see Supplement for description of J_{NO_2} measurements), independently for both setups. The flows of N_2, O_2, air and NO were set by mass flow controllers. The RH was set by a humidifier placed after the admission of N_2 and O_2 gases but before the admission of NO or NO_2 (see Fig. 1), in which the carrier gas bubbles through liquid water at a given temperature. The humidifier could also be bypassed to set a RH of near zero. A typical measurement sequence is described in Sect. 2.1.2.

The J_{NO_2} was measured for both Setup 1 and 2 using NO_2 actinometry. The J_{NO_2} with seven lamps was found to be $2 \times 10^{-2}\,s^{-1}$ for Setup 1 and $1 \times 10^{-2}\,s^{-1}$ for Setup 2 (see Fig. S1 for Setup 1 and Supplement text for both Setups). These values were compared to direct actinic flux measurements in the flow tube and thus normalized (see Sect. 3.1.1).

2.1.1 Flow tube instrumentation

The following gas-phase products exiting the flow tube were measured by three different instruments: NO_2 by the University of Colorado Light Emitting Diode Cavity-Enhanced Differential Optical Absorption Spectroscopy (LED-CE-DOAS) instrument (Thalman and Volkamer, 2010), HONO by a LOng Path Absorption Photometer (LOPAP, QuMA GmbH, Heland et al., 2001; Kleffmann et al., 2002) and NO by a chemiluminescence analyzer (Ecophysics CLD 77 AM, also used for NO_2 in Setup 2). HO_2 radicals were indirectly measured by detecting NO_2 with the LED-CE-DOAS (Setup 1) and by the loss of NO with the chemiluminescence detector (Setup 2). The latter was preceded by a molybdenum converter to transform HONO and NO_2 to NO and by an alkaline trap for HONO. Both trap and converter had a bypass to allow sequential measurements, thereby obtaining the concentration of NO_2 and HONO separately. HONO was measured by the LOPAP during some selected experiments (Kleffmann et al., 2002, 2006).

LED-CE-DOAS

The LED-CE-DOAS instrument (Thalman and Volkamer, 2010) detects NO_2 absorption at blue wavelengths. A high-power blue LED light source (420–490 nm) is coupled to a confocal high-finesse optical cavity consisting of two highly reflective mirrors ($R = 0.999956$) peaking at 460 nm that are placed about 87.5 cm apart (sample path length of 74 cm). The absorption path length depends on wavelength, and was about ~ 11 km near peak reflectivity here. A purge flow of dry nitrogen gas is added to keep the mirrors clean. The light exiting the cavity is projected onto a quartz optical fiber coupled to a Princeton Instruments Acton SP2156 Czerny-Turner imaging spectrometer with a PIXIS 400B CCD detector. The mirror reflectivity was calculated by flowing helium and nitrogen gas, exploiting the difference in the Rayleigh scattering cross sections of both gases as described in Thalman et al. (2014). The gas exiting the flow tube was directly injected into the CE-DOAS cavity, and spectra were recorded every 60 s and stored on a computer. For analysis we use broadband cavity enhanced absorption spectroscopy (BBCEAS) fitting at NO_2 concentrations exceeding a few parts per billion by volume (Washenfelder et al., 2008) and

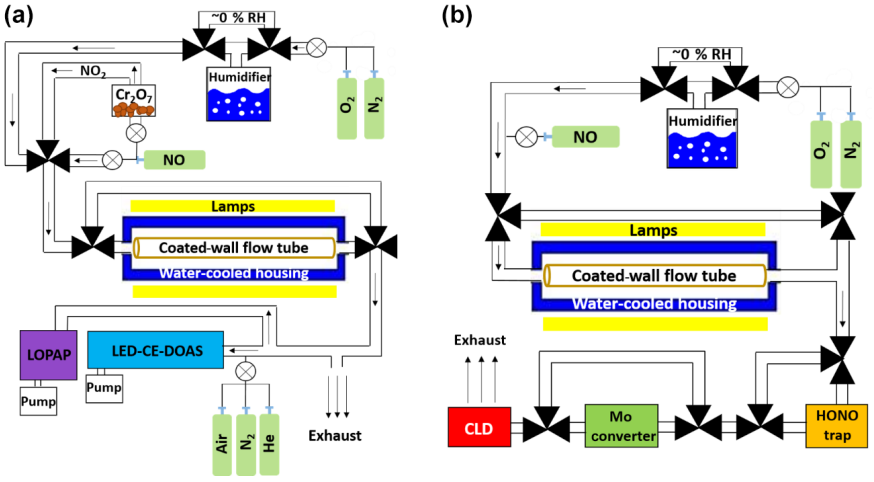

Figure 1. Sketch of the photochemical flow tube reactor setups at PSI for **(a)** Setup 1 in 2013 measuring NO_2 generation and **(b)** for Setup 2 in 2014 measuring NO loss.

DOAS least-squares fitting methods at lower concentrations (Thalman et al., 2015). The mirror alignment was monitored online as part of every spectrum by observing the slant-column density of oxygen collision complexes, O_2–O_2 (O_4) (Thalman and Volkamer, 2010, 2013). The following reference spectra were taken from the literature: NO_2 (Vandaele et al., 2002) and O_2–O_2 collision complexes (Thalman and Volkamer, 2013). The detection limit for NO_2 was 50–100 pptv.

2.1.2 Experimental conditions

The IC + CA solutions were prepared by adding IC into a 1 M CA solution in 18 MΩ cm ultrapure water to achieve IC to CA molecular ratios of between 0.026 and 0.127 in the film. The bulk solutions for both setups were prepared by weighing out 384–400 mg of CA in 2 mL of water and adding 4–20 mg of IC to the solution. The solutions for both setups were freshly prepared for each experiment, and the masses in the film were calculated at 50 % RH from the CA hygroscopic growth factors reported by Zardini et al. (2008) for both setups (for Setup 1: 5–18 mg of IC and 44 mg of CA; for Setup 2: 1–5 mg of IC and 77 mg of CA). The range of concentrations in the films was between 0.148 and 0.671 M of IC and 5.29 and 6.68 M of CA.

The IC + CA solution coatings were produced by depositing 220–250 (Setup 1) and 400 µL (Setup 2) of the desired solution in a Duran glass tube, which was then dispersed into a thin and viscous film of 3–4 µm. The film was dried with a gentle N_2 stream humidified to a RH similar to the experimental RH and room temperature. The film was rolled and turned upside down to deposit a homogenous film throughout the entire inner surface of the flow tube. The homogeneity of the film was confirmed by visual inspection. If a bright clear homogenous amorphous film from the supercooled solution was not observed, the film was discarded (e.g., observation of a turbid and cracked crystallized appearance). The carrier gas flows consisted of premixed dry N_2 and O_2 (a ratio of 4.5 / 1 in Setup 1 and a ratio of 2 in Setup 2), and NO was controlled by mass flow controllers. The total flow rates were 500 mL min^{-1} for Setup 1 and 1500 mL min^{-1} for Setup 2. In Setup 1, a dilution flow of 1000 mL min^{-1} was added at the end of the flow tube for a total of 1500 mL min^{-1} during experiments when HONO was measured along with NO_2. All experiments were conducted at ambient pressure, leading to gas residence times of 2.1–2.4 s (depending on flow tube volume, for both setups) under laminar flow conditions. The O_2 flow rate was varied between 0 and 110 mL min^{-1} to observe the dependence of O_2 while keeping the total flow rate constant. A ratio of 4.5 : 1 of N_2 : O_2 was maintained if any of the other gas flows were changed (e.g., NO and/or NO_2) for Setup 1. For Setup 2, a ratio of 2 : 1 of N_2 : O_2 was also maintained, except for the O_2 concentration dependence studies. The RH was kept constant at 50 % RH during most experiments and varied between 10 and 60 % RH to study humidity effects of the HO_2 radical production. The concentration of NO was ∼ 1 ppmv (Setup 1) and varied between 100 and 500 ppbv (Setup 2). Scavenging of HO_2 was achieved by the following reaction:

$$NO + HO_2 \rightarrow NO_2 + OH. \quad (R1)$$

The lifetime of HO_2 is about 5 ms when 2.5×10^{13} molecules cm^{-3} of NO are present (Setup 1), which ensures efficient conversion of HO_2 molecules into NO_2 ($k = 8.0 \times 10^{-12}$ cm^3 molecule^{-1} s^{-1} at 298 K; Sander et al., 2011). As shown in Fig. S2, 500 ppbv NO, the concentration used in Setup 2, was sufficient to efficiently convert HO_2 into NO_2; see Sect. 3.1.1. The lifetime of gas-phase HO_2 with respect to loss to the organic film is about 0.1 s, based on a similar formula shown in Eq. (S3),

where $\gamma = 10^{-3}$ (upper limit by Lakey et al., 2015). Note that in view of the essentially diffusion-controlled loss of HO_2 to the CWFT and tubing walls, the chosen scheme for determining the production of HO_2 radicals from the films by fast scavenging with NO is superior to a more selective detection method, e.g., laser-induced fluorescence (LIF), which would require passing the HO_2 radicals into a separate setup with substantial losses. For selected experiments, the films were exposed to UV irradiation for over 6 h which showed only a minor change in the decrease in NO_2, leading to the conclusion that the reactivity of the films was stable.

2.1.3 J_{IC} calculations

The absorption cross section of IC and the calculated photolysis rate are shown in Fig. S3. The photolysis frequencies of IC were calculated using a similar procedure as described in Schwarzenbach et al. (2002). The spectral actinic flux in the flow tube, $F_{FT}(\lambda)$, was converted to the spectral photon flux density that reaches the film in the flow tube, $F_{film}(\lambda)$, and the photon flux absorbed by IC, F_a^{IC}, as follows:

$$F_a^{IC} = \int_{300}^{420} F_{film}(\lambda) \times [1 - 10^{-\sigma_{IC}(\lambda) \times b \times C_{IC}}] d\lambda, \quad (1)$$

$$\text{where } F_{film}(\lambda) = \frac{F_{FT}(\lambda) \times SA}{N_a \times V_{film}},$$

where F_a^{IC} has units of Ein L^{-1} s^{-1} (1 Ein = 1 mole (6.022×10^{23}) of photons), $F_{film}(\lambda)$ has units of Ein L^{-1} s^{-1} nm^{-1}, b is the optical path length taken as the thickness of the film in cm, C_{IC} is the concentration of IC in the film in units of M, and σ_{IC} is the IC absorption cross section. The absorption spectrum of IC in water was based on the measurements by Kampf et al. (2012) and renormalized to the peak value of $10\,205 \pm 2400$ M^{-1} cm^{-1} at 284 nm (Maxut et al., 2015). V_{film} is the volume of the film in cm^3, calculated from the deposited mass of CA and the hygroscopic growth factors of CA (Zardini et al., 2008); SA is the surface area of the film, taken as the geometric area of the inner surface area of the flow tube in cm^2; N_a is Avogadro's number in molecules $mole^{-1}$. The IC photoexcitation rate J_{IC} was about 1.0×10^{-3} s^{-1} (upper limit).

We have also attempted to calculate an effective quantum yield for the formation of gas-phase HO_2 radicals (ϕ_{HO_2}):

$$P_{HO_2} = \frac{[NO_2] \times \text{flow}}{N_a \times V_{film}} \phi_{HO_2} = \frac{P_{HO_2}}{F_a^{IC}}, \quad (2)$$

where P_{HO_2} is the HO_2 production rate in mol L^{-1} s^{-1}, F_a^{IC} is the calculated mean absorbed photon flux by IC (Eq. 1), $[NO_2]$ is the gas-phase concentration of NO_2 in molecules cm^{-3} assuming a 1 : 1 ratio to HO_2 conversion, flow is the volumetric gas flow at the temperature in the CWFT and atmospheric pressure in cm^3 s^{-1} and V_{film} is in L.

2.1.4 Aerosol flow-reactor experiments

A detailed description of the aerosol flow tube (AFT) is reported elsewhere (Monge et al., 2012; Aregahegn et al., 2013); therefore, only some principles are given below. The SOA experiments were conducted in a horizontal, cylindrical Pyrex aerosol flow reactor (13 cm i.d., 152 cm length) surrounded by seven UV lamps (Philips CLEO, 80W) with a continuous emission spectrum ranging from 300 to 420 nm (total irradiance of 3.31×10^{16} photons cm^{-2} s^{-1}). The flow reactor consisted of Teflon stoppers and different flow controllers that maintained the gas–aerosol–UV irradiation contact time between 20 and 50 min. This flow reactor also consisted of an outer jacket that controlled the temperature at 293 ± 2 K by water circulation using a thermostat (Model Huber CC 405).

Seed aerosols (50 nm) were produced by nebulizing a solution (at pH 6) containing ammonium sulfate (AS, 0.95 mM) and IC (1.3 mM), size selected by a DMA and exposed to gas-phase limonene (500 ppbv) in the aerosol flow reactor. The typical aerosol mass loading in the reactor was 2–3 µg cm^{-3}, corresponding to $\sim 15\,000$ particles cm^{-3} with a starting diameter of 50 nm. As shown by Aregahegn et al. (2013), limonene is an efficient H-donor VOC that forms SOA via reactive uptake to IC-containing seed aerosol. Due to the excess of limonene and low seed aerosol surface area, the consumption of limonene was below the detection limit. The aerosol growth was measured by means of an ultrafine condensation particle counter (UCPC) and a scanning mobility particle sizer spectrometer (SMPS; both TSI), and similarly to the CWFT experiment, a flow of gaseous NO (from a 1 ppmv cylinder, Linde) was added to the carrier gas, and its conversion to NO_2 was monitored by a chemiluminescence detector with a detection limit of 0.05 ppbv (ECO PHYSICS CLD 88). Due to the long residence time, the NO_2 concentration is affected by its photolysis in the AFT. As discussed below, P_{HO_2} was calculated, in this case, from the growth of the particle diameter measured at the exit of the flow tube; the assumption is that growth was due to reactive uptake of limonene only and that each limonene forms one HO_2 radical. At 30 ppbv NO, the HO_2 radical lifetime is around 2 s.

2.1.5 Experimental conditions

The total flow rate in the aerosol flow reactor was between 400–1000 mL min^{-1}, ensuring laminar flow conditions. The RH was varied between 0 and 50 %. The RH of particles in the flow reactor was controlled by saturating the carrier gas via a bubbler containing ultrapure water (Milli Q, 18 MΩ cm). The RH in the flow-reactor system was varied by changing the gas flow rates to the bubbler and the temperature of the circulating water jacket of the bubbler. The RH was measured with a humidity sensor (Meltec UFT 75-AT, Germany) at the exit of the flow reactor. The concentrations

for the flow tube experiments were the following: 30 ppbv of NO and 500 ppbv of limonene.

2.2 Chemicals

The following chemicals were used without further purification for CWFT studies: IC (97 %, Sigma Aldrich) and CA (Sigma Aldrich). For Setup 1, the Duran glass tubes were soaked in a deconex® cleaning solution overnight; the next day they were rinsed with 18 MΩ cm water (Milli Q Element system). These flow tubes were etched with a 5 % hydrofluoric acid solution after the washing procedure and again rinsed with water before any experimental use. The Duran flow tubes for Setup 2 were not initially etched with any acid but stored in a NaOH solution after washing and lastly rinsed with water; Setup 2 later confirmed that the treatment of flow tube with acids affects P_{HO_2} by rinsing with HCl and etching with HF solutions.

For the aerosol flow-reactor experiments, gas-phase limonene was generated from commercially available limonene (Aldrich, 97 %) by means of a permeation tube. The following chemicals were used without further purification: IC (97 %, Sigma Aldrich) and succinic acid (Sigma Aldrich, ≥ 99.5 %); 4-benzoylbenzoic acid (4-BBA, Aldrich 99 %) and adipic acid (AA, Aldrich, ≥ 99.5 %) were used to expand the CWFT studies to other photosensitizers.

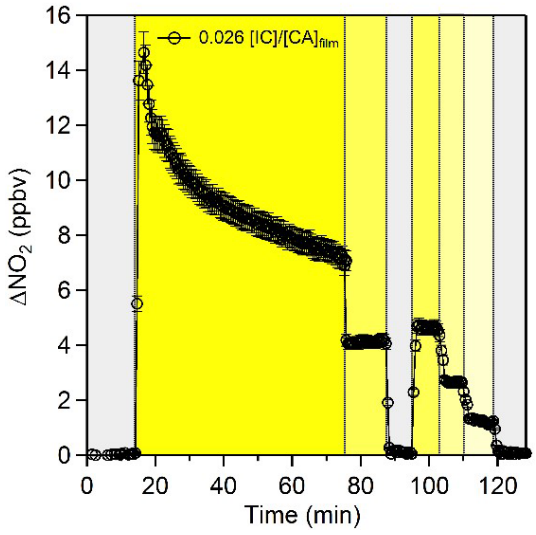

Figure 2. NO_2 profile for a 0.025 M IC bulk solution, whose concentration increases to ∼ 0.2 M of IC in the film due to the citric acid hygroscopic properties. The gray shaded areas indicate periods where NO was exposed in the dark. The yellow shaded areas indicates the period of irradiation; the decrease in the intensity of yellow represents 2.26×10^{16}, 1.47×10^{16}, 1.14×10^{16} and 3.94×10^{15} photons cm^{-2} s^{-1} for seven, five, three and one lamp, respectively. This time series clearly indicates the light dependence production of HO_2 radicals from the photosensitization of IC in a CA film.

3 Results and discussion

3.1 Coated-wall flow tube

The following results represent the light-dependent formation of HO_2 indirectly from measurements of NO_2 production and NO loss, measured with Setup 1 and 2, respectively. Figure 2 shows a time series of NO_2 measured with Setup 1 as a function of UV-A light, which confirms the light-dependent radical production. This particular film had an IC / CA ratio of 0.026 (0.148 M IC and 5.77 M CA in the film). An evident increase in NO_2 is observed upon UV irradiation, directly reflecting the light-mediated release of HO_2, as shown in Reaction (R1). The NO_2 signal decreases over time with all seven lamps; this was a common feature observed in all films and could be due to HO_2 sinks in the film increasing with time. Thus, the system only slowly evolves into a steady state. A small amount of NO_2 (0.5–1.5 ppbv) was observed during experiments that used only CA in the absence of IC; therefore, the data in Fig. 2 and all data reported below have been corrected for this NO_2 background, measured routinely in between experiments. Figure 2 also indicates a strong correlation with light intensity, which is further discussed in the context of Fig. 4. For irradiation, humidity and oxygen dependence experiments, each data point represents a separate experiment using a freshly prepared coated film in the flow tube. The uncertainty for experiments was based on the standard deviation of n, the number of experiments. The total uncertainty was ±6–27 % (propagated error for normalization was ±7–29 %) for the IC mass loading experiments in Setup 1 and up to a factor of 2 for the light dependence experiments. The uncertainty in Setup 2 was 10–50 %. As discussed earlier, the lifetime of HO_2 in the system was about 3 orders of magnitude less than the residence time in the flow tube, therefore suggesting that most, if not all, HO_2 reacted with NO to produce the observed NO_2 (Reaction R1). Theoretically, the system was clean of other oxidants such as O_3 (and thus NO_3). The uptake of NO_2 in the film was too small to further produce any nitrate radicals, and the photolysis of NO_2 in the experiments to produce O_3 was insignificant (< 1 %). The recombination of NO and O_3 contributes a negligible (< 0.1 %) NO_2 source under our experimental conditions. RO_2 generation from the reaction between CA and OH from HONO photolysis was also ruled out since it is approximated to account for only 1 % of the NO_2 production if we assume every OH from the photolysis reacts with CA. To our knowledge, the direct photolysis of CA to produce any RO_2 radicals has not been observed. Therefore, we believe that HO_2 is the essential oxidant for NO and refer to the measured NO_2 as HO_2 formation.

Figure 3 shows that the HO_2 production fluxes, in molecules cm^{-2} min^{-1}, increased with IC mass loading. The CA concentration was kept constant, and results are shown as the product between [IC] × [CA], since we expect that the

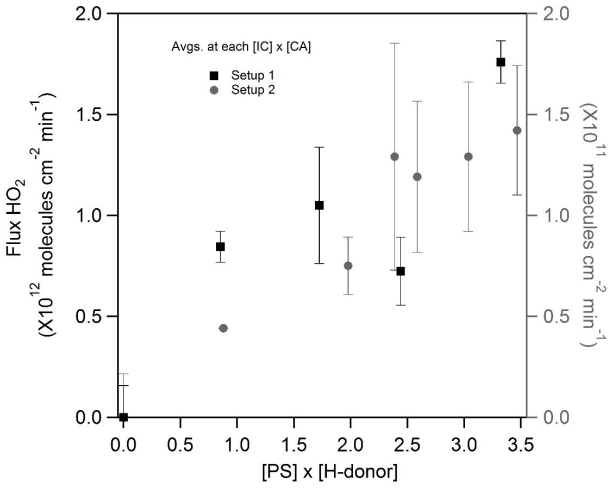

Figure 3. A linear correlation of HO_2 as a function of IC concentration. The left *y* axis represents the values for Setup 1, while the right *y* axis represents the values for Setup 2 (an order of magnitude difference for both scales). The Setup 2 data fall between a factor of 2 and 3 from Setup 1 after accounting for differences between Setup 1 and 2; see Sect. 3.1.1.

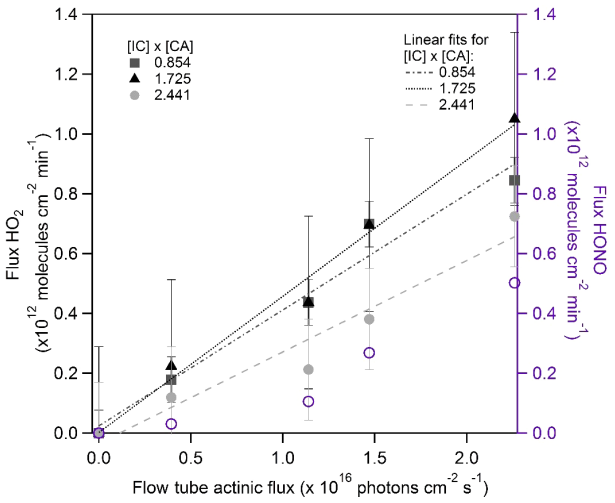

Figure 4. HO_2 fluxes in molecules cm^{-2} min^{-1} as a function of actinic flux for a 300–420 nm range (solid symbols). The data are plotted as a concentration product of [IC] × [CA] (shown in the legend), which shows the photochemical reaction between IC and CA in H_2O matrix and gaseous NO. HONO for 2.441 ([IC] × [CA]) is plotted on the right axis (open circles), showing a ratio of $HONO : NO_2 < 1$, which suggests OH as a secondary product.

production rate of HO_2 is proportional to the concentration of IC, at constant illumination, and to that of the potential H donor, CA. For Setup 1, the HO_2 fluxes were measured as NO_2 mixing ratios and calculated using the following equation:

$$\text{Fluxes}_{HO_2} = \frac{[NO_2] \times \text{flow}}{\text{SA}}. \quad (3)$$

The description of these parameters has been previously explained (see Sect. 2.1.3). For Setup 2, the HO_2 flux was calculated similarly, but only about half of the observed NO loss was considered to account for the loss of NO via the reaction with OH (see Reaction R1 in Supplement), meaning that for each HO_2 scavenged, two NO molecules were lost. In Fig. 3, the data from Setup 1 are represented by the black squares and the data from Setup 2 are represented by the gray circles. Setup 1 measurements were taken at about ∼ 50 % RH and at room temperature. Setup 2 measurements were taken at 45 % RH and at 292 K. Temperature has an effect on the observed gas-phase HO_2 release from the film and thus needs to be accounted for, which is not done in Fig. 3, but it is described in detail in Sect. 3.1.1.

Figure 4 shows that the HO_2 production exhibited a linear dependence on the actinic flux for various [IC] × [CA] molar products. From Sect. 2.1.3, we estimated an experimental ϕ_{HO_2} of about 6×10^{-5}, reflecting other probable, unknown quenching processes in our system. Figure 4 also shows the formation of HONO from three different IC mass loadings. In all three cases, the $HONO : NO_2$ ratio is < 1, confirming HO_2 as a primary product and OH as a secondary product.

Figure 5 shows the dependence of HO_2 production observed via the loss of NO (Setup 2) on relative humidity (0–65 %). Water partial pressure is an important parameter in the atmosphere, and it also seems to have an important effect on the photochemical reactions studied here. At RH below ∼ 10 %, and at high RH above ∼ 55 %, the yield of HO_2 radicals decreases. The maximum HO_2 radical production is observed at moderate RH (20–55 %). This is probably due to a combination of factors. In particular, at low RH the film may become more viscous, reducing mobility and thus the energy transfer within the film. This may decrease the HO_2 yield as shown in Fig. 5. Hinks et al. (2016) observed that the movement of molecules in a viscous film at a low RH is hindered and thus decreases the photochemical reaction rate of secondary organic material. The reduced diffusivity of HO_2 may also increase the residence time in the film and facilitate the self-reaction in the bulk phase: the diffusivity of H_2O in citric acid is in the range of 10^{-7}–10^{-8} cm^2 s^{-1} at 50 % RH. If the HO_2 diffusivity is between a factor of 10 and 100 lower than that of H_2O due to its larger size (10^{-9} cm^2 s^{-1}), the first-order loss rate coefficient for diffusion out of the film (D / δ^2, δ denoting the film thickness (4×10^{-4} cm)) becomes about $k_D = 10^{-2}$ s^{-1}. From the observed F_{HO_2}, the steady-state concentration is then about $F_{HO_2}/k_D/\delta = 4 \times 10^{16}$ $cm^{-3} = 10^{-7}$ M. The loss rate coefficient due to HO_2 self-reaction in the condensed phase (7.8×10^5 M^{-1} s^{-1}) at this concentration would become nearly 0.1 s^{-1}, somewhat higher than that for diffusional loss. Of course these estimates carry a high uncertainty but indicate that at lower humidity, diffusivity gets low enough to effectively reduce the diffusional loss of HO_2 to the gas phase and favor its loss by self-reaction in the con-

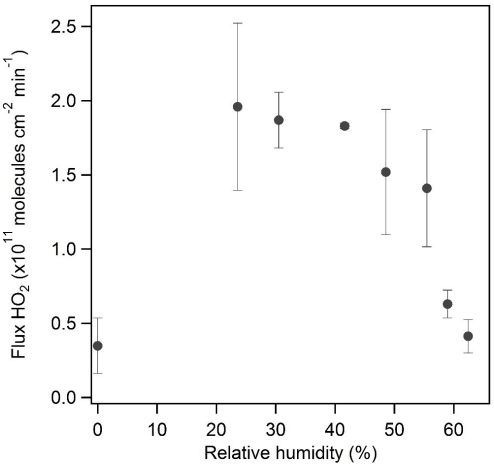

Figure 5. The indirect flux of HO_2 in molecules cm^{-2} min^{-1}, measured by NO loss and normalized to the film surface area as a function of relative humidity.

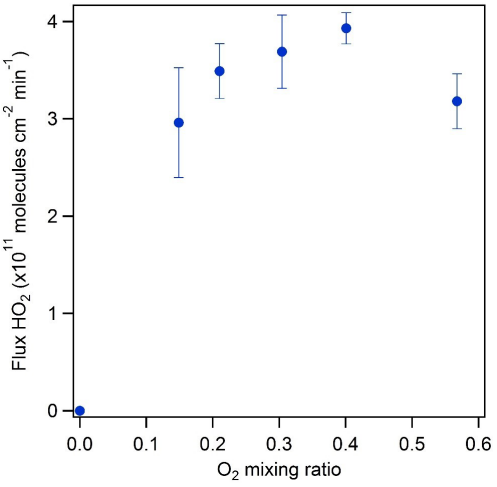

Figure 6. The flux of HO_2 in molecules cm^{-2} min^{-1}, measured by NO loss, above a film composed of IC and CA normalized to the film surface area as a function of the O_2 mixing ratio.

densed phase. The potential presence of condensed phase sinks, such as RO_2, formed from secondary chemistry of oxidized citric acid, may add to this uncertainty. Figure S4 shows that bulk diffusion can be neglected since any HO_2 produced below the first couple of micrometers at the top of the film is likely lost to self-reaction in the condensed phase. This supplementary experiment studied the thickness dependence of the films keeping the IC : CA ratio constant. The results show that P_{HO_2} increases linearly with thickness up to $\sim 2.5\,\mu m$; however, after this thickness the film saturates, showing that this must happen in our films that are between 3 and 4 µm thick. At high RH ($> 55\,\%$), the amount of water associated with CA dilutes the reactants, and the quenching of the excited IC triplet states gains in relative importance, consistent with findings in other studies (Stemmler et al., 2006, 2007; Jammoul et al., 2008). The RH effect can decrease the HO_2 production by a factor of 3, compared to the plateau of maximum HO_2 production between 20 and 55 % RH.

Figure 6 shows the dependence of the HO_2 production based on the observed NO loss on the O_2 mixing ratio (Setup 2). The HO_2 production varied by about 20 % over the range of conditions investigated. A decrease below 15 % O_2 appears to be significant compared to the maximum HO_2 production at $\sim 40\,\%$ O_2, indicating that O_2 is needed for HO_2 formation. Sufficient O_2 dissolves in the aqueous phase to produce HO_2 radicals efficiently at atmospheric O_2 mixing ratios. We assume that at 55 % O_2, the quenching of excited IC triplet states by O_2 has an effect on HO_2 production. This effect may decrease P_{HO_2} based on our results being qualitatively consistent with the observations of decreasing aerosol growth at high O_2 in the autophotocatalytic aerosol growth described in Aregahegn et al. (2013). However, the experimental focus of this study was based on atmospheric O_2 mixing rations, and thus we cannot draw conclusions about the HO_2 production at high O_2 mixing ratios.

In order to test the possibility for excited IC triplet states to react with NO_2 at the surface of the film, experiments were conducted with NO_2. While we did observe that the uptake of NO_2 on irradiated surfaces scaled with light intensity (see Fig. S5), the reactive uptake coefficient of NO_2 to produce HONO at the surface is rather small ($< 2.5 \times 10^{-7}$), corresponding to a k_w of $10^{-3}\,s^{-1}$, and is thus neither a significant loss of NO_2 nor a significant source of HONO. The primary fate of the nitrogen-containing aromatic alkoxy IC radical under atmospheric conditions is reaction with O_2. However, we have not tested alternative quenching reactions of the triplet state or other pathways of the reduced ketyl radical that do not result in the formation of HONO.

3.1.1 Comparison of data sets

The experimental conditions probed differ in the actinic flux, NO concentration, temperature and acidity. Here, we use the dependencies established in Sect. 3.1 to compare results from both setups. The data from Setup 2 were normalized to conditions of Setup 1. The difference in J_{NO_2} corresponds to multiplying results from Setup 2 with a factor of 2.0 ± 0.1. HO_2 was measured indirectly by reacting it with NO, and Fig. S2 indicates that the minimum NO concentration needed to efficiently scavenge all gas-phase HO_2 is ~ 460 ppbv of NO, indicating efficient conversion for Setup 1 and a conversion efficiency of ~ 0.6 for Setup 2. The data from Setup 2 were multiplied by 1.66 ± 0.10 to normalize for the NO conversion efficiency (Fig. S2) and by an additional factor of 1.25 ± 0.10 to match temperatures. We observed some limited variability depending on whether HF or HCl were used to clean the flow tube prior to experiments. A higher P_{HO_2}

was observed when cleaning with HF (Setup 1) compared to storing in NaOH and either rinsing with water or HCl (Setup 2); this is accounted for by multiplying data from Setup 2 with a factor of 1.25 ± 0.30. Notably, the error of the correction for the cleaning procedure that is propagated here is larger than the correction factor. The effect of the pretreatment of the flow tubes was not systematically studied and thus remains a primary uncertainty in the comparison. No further correction was applied for slight differences in RH. The overall correction factor amounts to 5.2 ± 1.4, with the error reflecting the propagated uncertainty. This explains most of the difference in P_{HO_2} between both setups. The normalized results agree within a factor of 2, which is a reasonably good agreement.

3.1.2 Extension to other photosensitizers

A limited number of experiments were performed using the CWFT approach, using 4-BBA as a photosensitizer, in the presence of 790 ppbv of gaseous limonene (a possible H donor) and NO. The organic thin film contained an organic acid matrix made of 4-BBA with and without adipic acid (AA). A substantial conversion of NO into NO_2 was also observed in this system (see Fig. S6). That 4-BBA behaves similar to the IC system demonstrates that the chemistry discussed above can occur on different excited carbonyls. It is interesting to note that this photoinduced conversion, and HO_2 production, was observed to be sustained over long times, i.e., more than 15 h, probably due to the catalytic nature of the underlying chemical cycles. However, a fraction of the IC did get consumed by photolysis reactions that do not form the excited triplet state (observed during overnight experiments). The HO_2 flux for the 4-BBA system was estimated to be 2.77×10^{10} molecules cm^{-2} min^{-1} making the same assumption that each HO_2 molecule reacts with NO to generate an NO_2 molecule. The calculation is based on Eq. (3), where it depends on the concentration of NO_2 as well as the surface area and residence time.

3.2 Aerosol flow tube

The aerosol flow tube experiments were conducted similarly to the study by Aregahegn et al. (2013), i.e., who demonstrated that in the absence of NO and known gas-phase oxidants, seed particles containing IC can initiate SOA growth in the presence of a gaseous H donor (limonene). Figure 7 shows the results from similar experiments when NO was added to the system. No conversion of NO to NO_2 was observed prior to the injection of limonene into the flow tube. The presence of a gaseous H donor and light clearly initiated a series of photochemical processes, leading to SOA growth and gaseous NO_2 production. However, the quantitative interpretation of these experiments is not straightforward due to efficient radical cycling in the VOC–NO_x–light photochemical system and the lack of a blank experiment

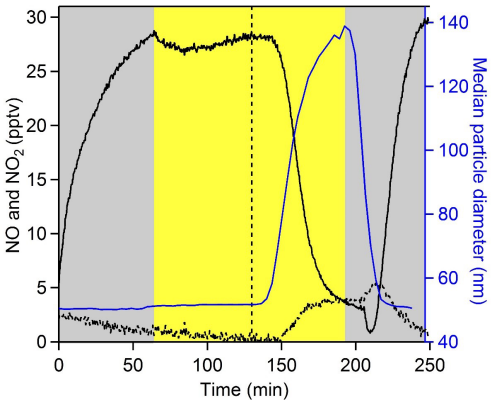

Figure 7. Aerosol flow tube experiments show rapid conversion of NO (solid black line) into NO_2 (dashed black line) only after the time when limonene (gaseous H donor) is added into the flow tube (vertical dashed line). The gray shaded areas represent the experiment in the dark, and the yellow shaded area represents the experiment under light exposure. The blue line represents the growth of aerosols (right axis).

that did not contain IC as part of the seed particles. Limitations arise from the much longer residence time, which allows NO_2 to be significantly photolyzed. The J_{NO_2} was estimated as $\sim 6.75 \times 10^{-3}$ s^{-1} and corresponds to a photolysis lifetime of 2.5 min, which is smaller than the actual residence time in the flow tube ($\sim$ 40 min). Secondary chemistry can lead, among others, to ozone production (O_3 lifetime at 500 ppbv limonene is $\sim$ 7 min) and secondary OH radical formation from the ozonolysis of limonene. Notably, NO_x is not consumed in Fig. 7. The overall effect of this secondary chemistry is an increased SOA growth compared to an experiment without added NO (Aregahegn et al., 2013). As a consequence, the NO_2 yield cannot be used directly to assess P_{HO_2} in the presence of NO.

However, in the absence of NO these secondary processes can largely be avoided and are reduced to a level at which they cannot be identified (Aregahegn et al., 2013). Under such conditions, the particle growth rates presumably carry information about the photosensitizer cycling and subsequent HO_2 production. If we assume one molecule of limonene reacts to produce one HO_2, the volume change of aerosols is proportional to the overall number of HO_2 produced. For example, a growth of 15 000 particles cm^{-3} from diameter 51.4 to 68.5 nm in 40 min (residence time) is equal to a P_{HO_2} of 1.67×10^{14} molecules cm^{-2} min^{-1}. This should be interpreted as an upper limit for the actual P_{HO_2} because water uptake may also be contributing to the volume growth. However, compared to the CWFT experiments the much higher surface-to-volume ratio of nanoparticles is expected to enhance the chemical coupling of a gas-phase H donor and the excited IC triplet state at the aerosol surface. This is at least in part deemed responsible for the 2 orders of magnitude higher P_{HO_2} in the aerosol flow tube compared to the CWFT exper-

iments. Notably, even if ϕ_{HO_2} in the aerosol flow tube was 2 orders of magnitude higher than in the CWFT, it is still significantly smaller than unity.

Primary HO_2 formation from IC

One of the main advantages of the CWFT is that it operates at a much shorter residence time. From Setup 1, we derive a P_{HO_2} of 1.76×10^{12} molecules cm^{-2} min^{-1} for IC / CA = 0.1 and $J_{NO_2} = 8 \times 10^{-3}$ s^{-1}. This corresponds to 2.9×10^4 molecules cm^{-3} s^{-1} once normalized by aerosol surface area (1.18×10^{-6} cm^2 cm^{-3}) and J_{NO_2} in the aerosol flow tube. Such a primary radical flux is equivalent to the OH radical production rate resulting from photolysis of ~ 1 pptv of HONO in the aerosol flow tube. Conversely, a P_{HO_2} of 1.67×10^{14} molecules cm^{-2} min^{-1} is equivalent to the OH radical production rate from ~ 100 pptv HONO in the aerosol flow tube. We conclude that seed particles containing IC contribute significantly (equivalent to 1–100 pptv HONO) to the primary HO_x radical production rate in the aerosol flow tube experiments in the presence of NO (Fig. 7). Primary HO_2 radicals formed from IC-containing seed particles react rapidly with NO to form OH radicals under the conditions shown in Fig. 7. The H-donor species is further expected to form primary RO_2 radicals. These primary HO_2 and RO_2 radicals add directly to the conversion of NO into NO_2 and indirectly by driving secondary NO-to-NO_2 conversion from the RO_2/HO_2 radical chain. The aerosol flow tube experiments thus qualitatively confirm the results obtained from macroscopic surfaces and highlight the potentially important role of surface-to-volume ratio and gaseous H donors to enhance the relevance of H-donor photochemistry as sources for HO_x–RO_x radicals and SOA.

3.3 Proposed mechanism

A mechanism that can describe the results from the CWFT experiments is shown in Fig. 8. It follows the mechanism first proposed by Canonica et al. (1995). The primary product in our system is the HO_2 radical, which forms from the reaction between a nitrogen-containing aromatic alkoxy IC radical and a ground-state oxygen molecule, recycling the IC molecule. The aromatic alkoxy radicals form from the excited triplet state of IC via transfer of an H atom from an H donor (in our case likely to be CA or the CA / H_2O matrix). While a fraction of the IC will get consumed by photolysis reactions that do not form the excited triplet state (see Sect. 3.1.2.), IC is also continuously produced from multiphase reactions, e.g., of glyoxal (Yu et al., 2011; Kampf et al., 2012; Maxut et al., 2015). Another conclusion is that OH is a secondary product. If OH was a first-generation product, we would have expected HONO : NO_2 ratios larger than 1 : 1. A smaller ratio was observed, as shown in Fig. 4, indicating that there was no direct evidence for primary formation of OH radicals. Interestingly, the H-donor species becomes activated as a result of H abstraction and can react further to produce organic peroxy radicals, as evidenced by the aerosol flow tube results.

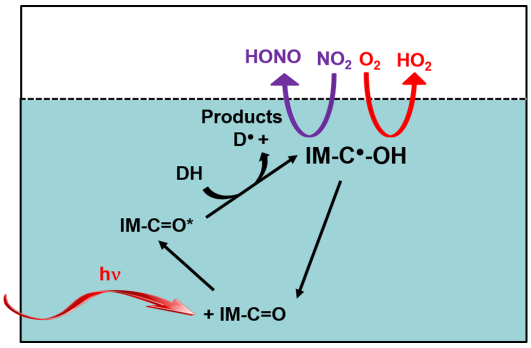

Figure 8. Proposed mechanism, modified and expanded to photosensitization of IC based on Canonica et al. (1995), George et al. (2005) and Aregahegn et al. (2013). The reaction in the white square represents the gas-phase, and the blue square represents the aqueous phase. DH is an H donor (e.g., CA, another IC, H_2O + CA matrix to be determined from flash photolysis).

4 Atmospheric relevance

The atmospheric relevance of our findings consists of the possible effect of heterogeneous radical sources to modify atmospheric HO_2 radical concentrations and facilitate aerosol growth and ageing by adding a radical source within aerosol particles. The production of HO_2 from IC photosensitized heterogeneous chemistry is a possible source of gas-phase HO_2 radicals in ambient air. In order to estimate the possible relevance for HO_2 radical concentrations in urban air, we assume P_{HO_2} of 2×10^{12} molecules cm^{-2} min^{-1} (IC / CA = 0.1, Setup 1) as a lower limit and 2×10^{14} molecules cm^{-2} min^{-1} (IC / AS = 0.1, aerosol flow tube) as an upper limit and typical conditions in Mexico City (i.e., $J_{NO_2} = 8 \times 10^{-3}$ s^{-1} at noontime in Mexico City, aerosol surface area = 15 cm^2 m^{-3}; Volkamer et al., 2007). The normalized P_{HO_2} during noontime in Mexico City ranges from 2×10^5 to 2×10^7 molecules cm^{-3} s^{-1}. This corresponds to a rate of new HO_x radical production of 4 to 400 pptv h^{-1} HONO around solar noon in Mexico City (Li et al., 2010), where other radical sources produce about 5.9×10^7 molecules cm^{-3} s^{-1} at solar noon (Volkamer et al., 2010). The upper range value suggests that aerosol surfaces can be a significant source of gas-phase HO_x in places like Mexico City. However, the IC molar ratios used here are likely an upper limit compared to ambient aerosols, yet, in principle other brown carbon molecules (i.e., HULIS and/or other imidazole derivatives) may form additional gas-phase HO_2. The heterogeneous HO_2 radical source could further be relatively more important in unpolluted regions under biogenic influences, where gas-phase radical production rates

are lower. Hence a more comprehensive characterization of the heterogeneous HO_2 source effect on gas-phase HO_2 radical concentrations deserves further investigation.

OH radical uptake from the gas phase is a primary OH source in aerosols (Ervens and Volkamer, 2010). Assuming a gas-phase OH concentration of 10^6 molecules cm^{-3}, 15 cm^2 m^{-3} aerosol surface area and γ_{OH} of unity, the rate of OH uptake is approximately 2.3×10^5 molecules cm^{-3} s^{-1}. The above estimated P_{HO_2} is a result from H transfer to form organic peroxy radicals, which is comparable to the rate of OH uptake. The two similar estimates of HO_x suggest that IC is a significant source of radicals in the condensed phase of particles. This is a lower limit due to the unknown radical losses of HO_x to the condensed phase, which have the potential to raise the HO_x source by up to a factor of 10 000 if limited by the IC excitation rate. The unknown amount of HO_2 that remains in the condensed phase is a further source of OH in the same phase; this OH, in the presence of reduced metals, can trigger a cycle of Fenton reactions or other oxidizing pathways that can further age the aerosol.

These results show that IC, and other aromatic carbonyl photosensitizers, are likely a relevant radical source in aerosol particles. Photoinduced radical generation in condensed phases is currently not represented in atmospheric models that describe aerosol ageing and warrants further study.

5 Conclusion

Three different experimental setups consistently show that HO_2 radicals are produced from the photochemistry of IC in a CA + H_2O matrix and in seed aerosols containing ammonium sulfate (in the presence of a gas-phase H donor, limonene). The linear correlations of P_{HO_2} (with [IC] / [CA] and irradiation) yielded maximum P_{HO_2} under atmospherically relevant irradiation, O_2 and RH but also revealed a complex role of film viscosity and possibly acidity effects (a systematic study of the effect of pH on the IC and CA absorption cross sections and the product yields from the IC photochemistry is desirable). If the H-donor species is in the condensed phase, significant amounts of HO_2 reach the gas phase only for moderately high RH ($\sim$ 25–55 % RH) that facilitates H transfer and allows molecules (IC, HO_2) to move freely towards the surface of the film. When the film is too dry, this mobility is inhibited due to enhanced viscosity and significantly decreases the P_{HO_2}. At RH and O_2 higher than 55 %, we observe a decrease in P_{HO_2} probably due to dilution by water and competing quenching reactions in the film. We know from Zardini et al. (2008) that pure citric acid does not efflorescence, and thus the film remains homogenous in its aqueous phase under all RH conditions. This supports our conclusion that the P_{HO_2} is RH dependent since it is partially controlled by the diffusivity in the film. On the contrary, if the H-donor species is in the gas phase, significant HO_2 production is also observed under dry conditions. The primary fate of the IC•-OH radical at the surface is reaction with O_2 to form HO_2. NO_2 reactions do not appear to form HONO at the surface. Our results suggest that the radical source from photosensitizers such as IC can help jump-start the photochemistry of VOCs. The effect on the gas-phase HO_2 radical concentration increases for higher surface-to-volume ratio of aerosols and in the presence of gas-phase H donors. The autophotocatalytic growth of aerosols containing photosensitizers via H-donor chemistry is an SOA source also in the presence of NO and adds oxidative capacity inside aerosol particles. Further research on other types of H donors and photosensitizers is necessary to compare different P_{HO_2} and rates of aerosol growth from the reactive uptake of VOC that could potentially have a significant atmospheric relevance for SOA formation and heterogeneous aerosol ageing.

6 Data availability

The data shown in the graphs are available in digital format (xlsx file) as part of the Supplement related to this article.

The Supplement related to this article is available online at doi:10.5194/acp-16-11823-2016-supplement.

Author contributions. Markus Ammann and Rainer Volkamer designed the experiments at PSI and Christian George and Barbara Nozière those at IRCELYON. Laura González Palacios, Pablo Corral Arroyo and Kifle Z. Aregahegn conducted the measurements, analyzed data and contributed equally to this work. Sarah S. Steimer and Thorsten Bartels-Rausch helped during the experiments, and all coauthors contributed to the data interpretation. Laura González Palacios and Rainer Volkamer prepared the manuscript with contributions from all coauthors.

Acknowledgements. This work was supported by the US National Science Foundation under awards ATM-847793 and AGS-1452317. Laura González Palacios is the recipient of a Chateaubriand Fellowship. Markus Ammann and Christian George appreciate the contribution by the EU project PEGASOS (EU–FP7 project under grant agreement no. 265307). This study has been supported by the Swiss National Science Foundation (grant 163074).

Edited by: D. Heard
Reviewed by: two anonymous referees

References

Aregahegn, K. Z., Nozière, B., and George, C.: Organic aerosol formation photo-enhanced by the formation of secondary photosensitizers in aerosols, Faraday Discuss., 165, 123–134, doi:10.1039/C3FD00044C, 2013.

Atkinson, R., Baulch, D. L., Cox, R. A., Crowley, J. N., Hampson, R. F., Hynes, R. G., Jenkin, M. E., Rossi, M. J., and Troe, J.: Evaluated kinetic and photochemical data for atmospheric chemistry: Volume I – gas phase reactions of O_x, HO_x, NO_x and SO_x species, Atmos. Chem. Phys., 4, 1461–1738, doi:10.5194/acp-4-1461-2004, 2004.

Badali, K. M., Zhou, S., Aljawhary, D., Antiñolo, M., Chen, W. J., Lok, A., Mungall, E., Wong, J. P. S., Zhao, R., and Abbatt, J. P. D.: Formation of hydroxyl radicals from photolysis of secondary organic aerosol material, Atmos. Chem. Phys., 15, 7831–7840, doi:10.5194/acp-15-7831-2015, 2015.

Calvert, J. G. and Pitts, J. N.: Photochemistry, Wiley, New York, 1966.

Canonica, S., Jans, U., Stemmler, K., and Hoigne, J.: Transformation Kinetics of Phenols in Water: Photosensitization by Dissolved Natural Organic Material and Aromatic Ketones, Environ. Sci. Technol., 29, 1822–1831, doi:10.1021/es00007a020, 1995.

Deguillaume, L., Leriche, M., Desboeufs, K., Mailhot, G., George, C., and Chaumerliac, N.: Transition metals in atmospheric liquid phases: sources, reactivity, and sensitive parameters, Chem. Rev., 105, 3388–3431, doi:10.1021/cr040649c, 2005.

Draper, W. M. and Crosby, D. G.: Photochemical generation of superoxide radical anion in water, J. Agr. Food Chem., 31, 734–737, doi:10.1021/jf00118a014, 1983.

Dupart, Y., King, S. M., Nekat, B., Nowak, A., Wiedensohler, A., Herrmann, H., David, G., Thomas, B., Miffre, A., Rairoux, P., D'Anna, B., and George, C.: Mineral dust photochemistry induces nucleation events in the presence of SO_2, P. Natl. Acad. Sci. USA, 109, 20842–20847, doi:10.1073/pnas.1212297109, 2012.

Ervens, B. and Volkamer, R.: Glyoxal processing by aerosol multiphase chemistry: towards a kinetic modeling framework of secondary organic aerosol formation in aqueous particles, Atmos. Chem. Phys., 10, 8219–8244, doi:10.5194/acp-10-8219-2010, 2010.

Ervens, B., Gligorovski, S., and Herrmann, H.: Temperature-dependent rate constants for hydroxyl radical reactions with organic compounds in aqueous solutions, Phys. Chem. Chem. Phys., 5, 1811–1824, doi:10.1039/b300072a, 2003.

Ervens, B., Turpin, B. J., and Weber, R. J.: Secondary organic aerosol formation in cloud droplets and aqueous particles (aqSOA): a review of laboratory, field and model studies, Atmos. Chem. Phys., 11, 11069–11102, doi:10.5194/acp-11-11069-2011, 2011.

Faust, B. C.: Aquatic Photochemical Reactions in Atmospheric, Surface, and Marine Waters: Influences on Oxidant Formation and Pollutant Degradation, in: Environmental Photochemistry, edited by: Boule, D. P., 101–122, Springer, Berlin Heidelberg, available at: http://link.springer.com/chapter/10.1007/978-3-540-69044-3_4 (last access: 7 December 2015), 1999.

Fenton, H. J. H.: LXXIII. Oxidation of tartaric acid in presence of iron, J. Chem. Soc. Trans., 65, 899, doi:10.1039/ct8946500899, 1894.

Galloway, M. M., Chhabra, P. S., Chan, A. W. H., Surratt, J. D., Flagan, R. C., Seinfeld, J. H., and Keutsch, F. N.: Glyoxal uptake on ammonium sulphate seed aerosol: reaction products and reversibility of uptake under dark and irradiated conditions, Atmos. Chem. Phys., 9, 3331–3345, doi:10.5194/acp-9-3331-2009, 2009.

George, C., Strekowski, R. S., Kleffmann, J., Stemmler, K., and Ammann, M.: Photoenhanced uptake of gaseous NO_2 on solid organic compounds: a photochemical source of HONO?, Faraday Discuss., 130, 195–210, 2005.

George, C., Ammann, M., D'Anna, B., Donaldson, D. J., and Nizkorodov, S. A.: Heterogeneous Photochemistry in the Atmosphere, Chem. Rev., 115, 4218–4258, doi:10.1021/cr500648z, 2015.

Heland, J., Kleffmann, J., Kurtenbach R., and Wiesen, P.: A new instrument to measure gaseous nitrous acid (HONO) in the atmosphere, Environ. Sci. Amp Technol., 35, 3207–3212, doi:10.1021/es000303t, 2001.

Hinks, M. L., Brady, M. V., Lignell, H., Song, M., Grayson, J. W., Bertram, A. K., Lin, P., Laskin, A., Laskin, J., and Nizkorodov, S. A.: Effect of viscosity on photodegradation rates in complex secondary organic aerosol materials, Phys. Chem. Chem. Phys., 18, 8785–8793, doi:10.1039/C5CP05226B, 2016.

Jacob, D.: Introduction to Atmospheric Chemistry, Princeton University Press, Princeton, N.J., 1999.

Jacob, R.: Entwicklung von chiralen- sowie RP-HPLC- Methoden in Verbindung mit hochaufloesender MS und deren Anwendung zur Analyse sekundaerer organischer Aerosole in der Atmosphaere, Doktor der Naturwissenchaften, Johannes Gutenberg-Universitaet Mainz, Mainz, Germany, 2015.

Jammoul, A., Gligorovski, S., George, C., and D'Anna, B.: Photosensitized Heterogeneous Chemistry of Ozone on Organic Films, J. Phys. Chem. A, 112, 1268–1276, doi:10.1021/jp074348t, 2008.

Kampf, C. J., Jakob, R., and Hoffmann, T.: Identification and characterization of aging products in the glyoxal/ammonium sulfate system – implications for light-absorbing material in atmospheric aerosols, Atmos. Chem. Phys., 12, 6323–6333, doi:10.5194/acp-12-6323-2012, 2012.

Kaur, R., Anastasio, C., Valsaraj, K. T., Vempati, H. S., and Vaitilingom, M.: Photoformation of Triplet Excited States and Other Oxidants in Fog Waters and Their Impact on Fog Processing of Organic Compounds, AGU Fall Meet. Abstr., 53, 07, 2014.

Kleffmann, J., Heland, J., Kurtenbach, R., Lörzer, J. C., and Wiesen, P.: A new instrument (LOPAP) for the detection of nitrous acid (HONO), Environ. Sci. Pollut. Res., 9, 48–54, 2002.

Kleffmann, J., Lörzer, J. C., Wiesen, P., Kern, C., Trick, S., Volkamer, R., Rodenas, M., and Wirtz, K.: Intercomparison of the DOAS and LOPAP techniques for the detection of nitrous acid (HONO), Atmos. Environ., 40, 3640–3652, doi:10.1016/j.atmosenv.2006.03.027, 2006.

Lakey, P. S. J., George, I. J., Whalley, L. K., Baeza-Romero, M. T., and Heard, D. E.: Measurements of the HO_2 Uptake Coefficients onto Single Component Organic Aerosols, Environ. Sci. Technol., 49, 4878–4885, doi:10.1021/acs.est.5b00948, 2015.

Li, G., Lei, W., Zavala, M., Volkamer, R., Dusanter, S., Stevens, P., and Molina, L. T.: Impacts of HONO sources on the photochemistry in Mexico City during the MCMA-2006/MILAGO Cam-

paign, Atmos. Chem. Phys., 10, 6551–6567, doi:10.5194/acp-10-6551-2010, 2010.

Maxut, A., Noziere, B., Fenet, B., and Mechakra, H.: Formation Mechanism and yield of small Imidazoles from Reactions of Glyoxal with NH_4^+ in water at neutral pH, Phys. Chem. Chem. Phys., 17, 20416–20424, doi:10.1039/C5CP03113C, 2015.

Monge, M. E., Rosenørn, T., Favez, O., Müller, M., Adler, G., Riziq, A. A., Rudich, Y., Herrmann, H., George, C., and D'Anna, B.: Alternative pathway for atmospheric particles growth, P. Natl. Acad. Sci., 109, 6840–6844, doi:10.1073/pnas.1120593109, 2012.

Monks, P. S.: Gas-phase radical chemistry in the troposphere, Chem. Soc. Rev., 34, 376–395, doi:10.1039/B307982C, 2005.

Nozière, B., Dziedzic, P., and Córdova, A.: Products and Kinetics of the Liquid-Phase Reaction of Glyoxal Catalyzed by Ammonium Ions (NH_4^+), J. Phys. Chem. A, 113, 231–237, doi:10.1021/jp8078293, 2009.

Rossignol, S., Aregahegn, K. Z., Tinel, L., Fine, L., Nozière, B., and George, C.: Glyoxal induced atmospheric photosensitized chemistry leading to organic aerosol growth, Environ. Sci. Technol., 48, 3218–3227, doi:10.1021/es405581g, 2014.

Sander, S. P., Abbatt, J., Barker, J. R., Burkholder, J. B., Friedl, R. R., Golden, D. M., Huie, R. E., Kolb, C. E., Kurylo, M. J., Moortgat, G. K., Orkin, V. L., and Wine, P. H.: Chemical Kinetics and Photochemical Data for Use in Atmospheric Studies, Evaluation No. 17, JPL Publ. 10-6, Jet Propulsion Laboratory, Pasadena, available at: http://jpldataeval.jpl.nasa.gov (last access: 8 August 2016) 2011.

Sareen, N., Schwier, A. N., Shapiro, E. L., Mitroo, D., and McNeill, V. F.: Secondary organic material formed by methylglyoxal in aqueous aerosol mimics, Atmos. Chem. Phys., 10, 997–1016, doi:10.5194/acp-10-997-2010, 2010.

Schwarzenbach, R. P., Gschwend, P. M., and Imboden, D. M.: Environmental Organic Chemistry, 2nd Edn., Wiley-Interscience, New York, 2002.

Shapiro, E. L., Szprengiel, J., Sareen, N., Jen, C. N., Giordano, M. R., and McNeill, V. F.: Light-absorbing secondary organic material formed by glyoxal in aqueous aerosol mimics, Atmos. Chem. Phys., 9, 2289–2300, doi:10.5194/acp-9-2289-2009, 2009.

Sheehy, P. M., Volkamer, R., Molina, L. T., and Molina, M. J.: Oxidative capacity of the Mexico City atmosphere – Part 2: A RO_x radical cycling perspective, Atmos. Chem. Phys., 10, 6993–7008, doi:10.5194/acp-10-6993-2010, 2010.

Stemmler, K., Ammann, M., Donders, C., Kleffmann, J., and George, C.: Photosensitized reduction of nitrogen dioxide on humic acid as a source of nitrous acid, Nature, 440, 195–198, doi:10.1038/nature04603, 2006.

Stemmler, K., Ndour, M., Elshorbany, Y., Kleffmann, J., D'Anna, B., George, C., Bohn, B., and Ammann, M.: Light induced conversion of nitrogen dioxide into nitrous acid on submicron humic acid aerosol, Atmos. Chem. Phys., 7, 4237–4248, doi:10.5194/acp-7-4237-2007, 2007.

Sumner, A. J., Woo, J. L., and McNeill, V. F.: Model Analysis of Secondary Organic Aerosol Formation by Glyoxal in Laboratory Studies: The Case for Photoenhanced Chemistry, Environ. Sci. Technol., 48, 11919–11925, doi:10.1021/es502020j, 2014.

Teich, M., van Pinxteren, D., Kecorius, S., Wang, Z., and Herrmann, H.: First Quantification of Imidazoles in Ambient Aerosol Particles: Potential Photosensitizers, Brown Carbon Constituents, and Hazardous Components, Environ. Sci. Technol., 50, 1166–1173, doi:10.1021/acs.est.5b05474, 2016.

Thalman, R. and Volkamer, R.: Inherent calibration of a blue LED-CE-DOAS instrument to measure iodine oxide, glyoxal, methyl glyoxal, nitrogen dioxide, water vapour and aerosol extinction in open cavity mode, Atmos. Meas. Tech., 3, 1797–1814, doi:10.5194/amt-3-1797-2010, 2010.

Thalman, R. and Volkamer, R.: Temperature dependent absorption cross-sections of O_2–O_2 collision pairs between 340 and 630 nm and at atmospherically relevant pressure, Phys. Chem. Chem. Phys., 15, 15371–15381, doi:10.1039/C3CP50968K, 2013.

Thalman, R., Zarzana, K. J., Tolbert, M. A., and Volkamer, R.: Rayleigh scattering cross-section measurements of nitrogen, argon, oxygen and air, J. Quant. Spectrosc. Ra., 147, 171–177, doi:10.1016/j.jqsrt.2014.05.030, 2014.

Thalman, R., Baeza-Romero, M. T., Ball, S. M., Borrás, E., Daniels, M. J. S., Goodall, I. C. A., Henry, S. B., Karl, T., Keutsch, F. N., Kim, S., Mak, J., Monks, P. S., Muñoz, A., Orlando, J., Peppe, S., Rickard, A. R., Ródenas, M., Sánchez, P., Seco, R., Su, L., Tyndall, G., Vázquez, M., Vera, T., Waxman, E., and Volkamer, R.: Instrument intercomparison of glyoxal, methyl glyoxal and NO_2 under simulated atmospheric conditions, Atmos. Meas. Tech., 8, 1835–1862, doi:10.5194/amt-8-1835-2015, 2015.

Trainic, M., Abo Riziq, A., Lavi, A., Flores, J. M., and Rudich, Y.: The optical, physical and chemical properties of the products of glyoxal uptake on ammonium sulfate seed aerosols, Atmos. Chem. Phys., 11, 9697–9707, doi:10.5194/acp-11-9697-2011, 2011.

Vandaele, A. C., Hermans, C., Fally, S., Carleer, M., Colin, R., Mérienne, M.-F., Jenouvrier, A., and Coquart, B.: High-resolution Fourier transform measurement of the NO_2 visible and near-infrared absorption cross sections: Temperature and pressure effects, J. Geophys. Res.-Atmos., 107, 4348, doi:10.1029/2001JD000971, 2002.

Volkamer, R., San Martini, F., Molina, L. T., Salcedo, D., Jimenez, J. L., and Molina, M. J.: A missing sink for gas-phase glyoxal in Mexico City: Formation of secondary organic aerosol, Geophys. Res. Lett., 34, L19807, doi:10.1029/2007GL030752, 2007.

Volkamer, R., Sheehy, P., Molina, L. T., and Molina, M. J.: Oxidative capacity of the Mexico City atmosphere – Part 1: A radical source perspective, Atmos. Chem. Phys., 10, 6969–6991, doi:10.5194/acp-10-6969-2010, 2010.

Washenfelder, R. A., Langford, A. O., Fuchs, H., and Brown, S. S.: Measurement of glyoxal using an incoherent broadband cavity enhanced absorption spectrometer, Atmos. Chem. Phys., 8, 7779–7793, doi:10.5194/acp-8-7779-2008, 2008.

Weller, C., Horn, S., and Herrmann, H.: Effects of Fe(III)-concentration, speciation, excitation-wavelength and light intensity on the quantum yield of iron(III)-oxalato complex photolysis, J. Photochem. Photobiol. Chem., 255, 41–49, doi:10.1016/j.jphotochem.2013.01.014, 2013a.

Weller, C., Horn, S., and Herrmann, H.: Photolysis of Fe(III) carboxylato complexes: Fe(II) quantum yields and reaction mechanisms, J. Photochem. Photobiol. Chem., 268, 24–36, doi:10.1016/j.jphotochem.2013.06.022, 2013b.

Yi, J., Bahrini, C., Schoemaecker, C., Fittschen, C. and Choi, W.: Photocatalytic Decomposition of H_2O_2 on Different TiO_2 Surfaces Along with the Concurrent Generation of HO_2 Radi-

cals Monitored Using Cavity Ring Down Spectroscopy, J. Phys. Chem. C, 116, 10090–10097, doi:10.1021/jp301405e, 2012.

Yu, G., Bayer, A. R., Galloway, M. M., Korshavn, K. J., Fry, C. G., and Keutsch, F. N.: Glyoxal in Aqueous Ammonium Sulfate Solutions: Products, Kinetics and Hydration Effects, Environ. Sci. Technol., 45, 6336–6342, doi:10.1021/es200989n, 2011.

Zardini, A. A., Sjogren, S., Marcolli, C., Krieger, U. K., Gysel, M., Weingartner, E., Baltensperger, U., and Peter, T.: A combined particle trap/HTDMA hygroscopicity study of mixed inorganic/organic aerosol particles, Atmos. Chem. Phys., 8, 5589–5601, doi:10.5194/acp-8-5589-2008, 2008.

Zellner, R., Exner, M., and Herrmann, H.: Absolute OH quantum yields in the laser photolysis of nitrate, nitrite and dissolved H_2O_2 at 308 and 351 nm in the temperature range 278–353 K, J. Atmos. Chem., 10, 411–425, 1990.

Zhao, R., Lee, A. K. Y., Soong, R., Simpson, A. J., and Abbatt, J. P. D.: Formation of aqueous-phase α-hydroxyhydroperoxides (a-HHP): potential atmospheric impacts, Atmos. Chem. Phys., 13, 5857–5872, doi:10.5194/acp-13-5857-2013, 2013.